This is the manuscript of the following published article:

E. Moradi, S. Amendola, T. Björninen, L. Sydänheimo, J. M. Carmena, J. M. Rabaey, L. Ukkonen, “Backscattering neural tags for wireless brain-machine interface,” *IEEE Trans. Antennas Propag.*, vol. 63, no. 2, pp. 719–726, Feb. 2015. DOI: 10.1109/TAP.2014.2384038

Published version is available in IEEE Xplore Digital Library:

http://ieeexplore.ieee.org/xpl/articleDetails.jsp?arnumber=6991545

Backscattering Neural Tags for Wireless Brain-Machine Interface Systems

Elham Moradi, *Student Member, IEEE,* Sara Amendola, *Student Member, IEEE,* Toni Björninen, *Member, IEEE,* Lauri Sydänheimo, *Member IEEE,* Jose M. Carmena, *Senior Member, IEEE,* Jan M. Rabaey, *Fellow IEEE,* Leena Ukkonen, *Member IEEE*

***Abstract*— Brain-machine interface (BMI) technology has tremendous potential to revolutionize healthcare by greatly improving the quality of life of millions of people suffering from a wide variety of neurological conditions. RFID-inspired backscattering is a promising approach to wireless powering of miniature neural sensors required in BMI interfaces. We analyze the functionality of mm-size loop antennas in the wireless powering of miniature cortical implants through measurements in a human head equivalent liquid phantom and in the head of a post-mortem pig. For the first time, we present the design and measurement of a miniature $1\times1\times1$ mm^3 backscattering device based on a cubic loop connected with an RFID IC. Our measurement results show that this very small loop receives sufficient electromagnetic power to activate the IC when the device is implanted in a pig's head. This demonstrates the feasibility of extremely small implant antennas in challenging wireless biomedical systems.**

***Index Terms*—backscattering neural sensor, near field inductive link, neural prostheses, wireless brain-machine interface**

I. Introduction

BRAIN-Machine Interfaces (BMI) is a young multidisciplinary field that has grown tremendously during the last decade [1]. BMI systems have enormous potential as a therapeutic technology that will improve the quality of life of millions of people suffering from spinal cord injury, stroke, amyotrophic lateral sclerosis, and other severely disabling neurological conditions. However, one of the main challenges in the development towards clinically viable BMIs is the lack of implantable technology that lasts for a life-time. Fully integrated, ultra-low power, wireless neural interfaces will play a key role in this endeavor [1−3].

The implanted BMI microsystems include neural-recording circuits to amplify and digitize the acquired neural signals. The implantability poses major constraints on the size and total power consumption of these systems. To monitor the electrical activity of the cortical neurons in various locations, high-channel-count recording systems are needed. However, the chip area per channel must be small so that the overall system exhibits a small form factor, which possibly permits the circuitry integration within the antenna layout [4]. Furthermore, the power consumption per channel must be minimal in order to keep the total amount of dissipated power within feasible limits for remotely-powered battery-less systems. Recent advances in the research on integrated-circuit (IC) technologies have decreased the chip area and power consumption per recording channel enabling hundreds of channels on a single chip.

Real-time signal processing platform would need to dissipate less than 10 μW/channel to allow completely wireless powering from an inductive link. Power requirements of some neural recording microsystems chosen among those recently reported in literature are listed below. The systems reported in [5−6] represent examples of neural recording devices with 32 and 128 channels, respectively, both requiring an averaged power per channel of 10 μW. An ECoG/EEG processing interface, which not only amplifies and conditions the signal, but also extracts sub-banded energy in multiple frequencies with 6.4 μW/channel power dissipation was presented in [7]. Authors of [8], proposed a complete chipset for a 100-channel wireless neural recording system whose neural interface requires 4.54 μW/channel. Even lower power consuming ICs are presented in [9−10]. The system reported in [9] achieved a very low average power consumption of 3.77 μW/channel. However, due to its very large area per channel, it may not be scalable to a high-channel-count system. An area-efficient double-channel neural acquisition system occupying 0.013 mm^2 while consuming 5 μW power was described in [10]. Besides the size and the power consumption, also the generated voltage at the IC terminals must be taken into account. As an example, the neural sensor system reported in [10] needs 0.5 V RF voltage amplitude at the rectifier for efficient RF-to-DC conversion.

In most of the solutions presented in the literature, power

Manuscript received February 18, 2014. This work was funded by Academy of Finland, Centennial Foundation of Finnish Technology Industries, Finnish Funding Agency for Technology and Innovation (TEKES), TUT Foundation, HPY Research Foundation, Nokia Foundation, and Sponsors of Berkeley Wireless Research Center and Brain-Machine Interface Systems Laboratory.

E. Moradi, T. Björninen, L. Sydänheimo, and Leena Ukkonen are with Tampere University of Technology, Department of Electronics and Communications Engineering, Finland (e-mail: elham.moradi@tut.fi).

J. M. Rabaey is with University of California at Berkeley, Berkeley Wireless Research Center (e-mail: jan@eecs.berkeley.edu).

J. M. Carmena is with the Department of Electrical Engineering and Computer Sciences and the Helen Wills Neuroscience Institute, University of California at Berkeley, (e-mail: jcarmena@berkeley.edu).

for the implant microsystem was supplied from a conventional or rechargeable battery. Battery-assisted implants increase the infection risk of the patient during surgery to replace the discharged battery. Recent work [11] demonstrated a fully implantable neural interface microsystem that obtained its power from a rechargeable battery and sent its acquired neural data to external unit through inductive link. However, the study reports a temperature increase during the charging mode of the battery [11]. Thus, wireless powering of the implant device is the solution to eliminate the need of a battery. When a dielectric material is placed in an electric field, electric charges shift from their equilibrium causing dielectric polarization. This consumes electric field energy producing heat in the dielectric material. Since human body tissues are highly dielectric, wireless power transfer through magnetic field allows efficient powering of the implant devices. Consequently, short range RFID backscattering technology using an inductive link is a promising solution to realize the wireless powering of and communication with the implant [12−13].

In an RFID-inspired backscattering system, an external interrogator transmits a carrier signal from which the implant antenna captures energy to power the implanted microelectronic system. The data link from the implant to the external interrogator is established through the modulation of the impedance terminating the implant antenna according to the acquired neurosignal. This extremely asymmetric system, where the complexity (and power consumption) is predominant at the interrogator, enables the implementation of ultra-low-power battery-free implants resembling RFID tags [3].

In this paper, we focus on the design and testing of miniature loop antennas for cortical implants and low profile external interrogator loop antennas. We have designed and tested mm-size implant loops providing strong enough coupling to an outside-body transmitter to establish wireless power and data telemetry in wireless BMI systems. The studied outside-body transmit loops allow transmission of hundreds of milliwatts of power while conforming Specific Absorption Rate (SAR) regulations. We have conducted measurements with the implant loops placed in a human head equivalent liquid phantom and in the head of a post-mortem pig.

II. Modeling of Wireless Link

Wireless link between an external transmit antenna and different types of implant antennas is modeled using ANSYS HFSS v. 15.05. In simulations, we used ANSYS Human Body Model (Man's Head) to model human tissues present in the wireless link between a neural sensor antenna and an external transmit antenna (Fig. 1). In our simulations, the implant antenna was immersed in the CSF fluid, which surrounds the brain. The external transmit antenna was placed 5 mm away from skin. Primary motor cortex area of the brain was chosen as the implant antenna site. Primary motor cortex elicits movements of individual body parts. Thus, neural reading and stimulation of this area is the target of BMI for thought-controlled smart prosthetics.

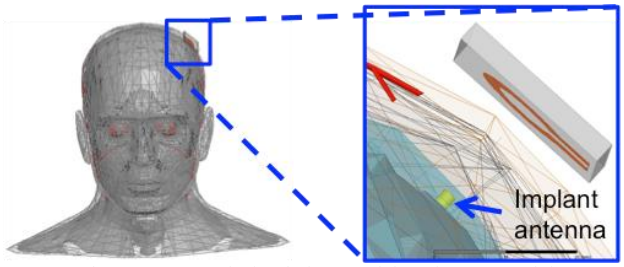

Fig. 1. The Man's Head simulation model and a zoomed image of transmit and implant antennas placed in the model.

Short range RFID backscattering technology can be implemented using near field inductive link. Efficiency and performance of inductive link can be analyzed by modeling it as a two-port network [14]. Thus, we characterized the link power efficiency between two loop antennas using the maximum operating power gain ($G_{p,max}$) of the two-port system. This is the ratio of the power delivered to the implant IC to the power supplied to the transmit antenna [15].

When transmitting power towards the human body, we must consider the exposure of the tissues to the electromagnetic field. According to FCC regulations, Specific Absorption Rate (SAR) averaged over a volume containing 1 g of tissue must be at or below 1.6 W/kg. Simulations showed that maximum SAR is generated in skin surface, which is the nearest tissue to the transmit antenna. We used the AverageSAR tool in HFSS, which calculates the SAR averaged over a volume containing 1 g of skin tissue surrounding each mesh point. In SAR simulations, we used a flat skin phantom. Then, we considered the maximum average SAR (SAR_{max}) for determining the maximum SAR-compliant transmit power ($P_{t,max}$):

$$P_{t,max} = \frac{1.6\ W/kg \times \tau_{S-ta}}{SAR_{max}} \times P_{t.} \tag{1}$$

Here P_t is the simulation test transmit power and $\tau_{S\text{-}ta}$ is the power transmission coefficient between the simulation test source and the transmit antenna. We computed the available power to the implant IC with the maximum allowed transmit power as [15]

$$P_L = G_{p,max} P_{t,max}. \tag{2}$$

This power would be delivered to an implant IC which is conjugate-matched with the implant antenna. Since the implant antenna is inductive, matched condition can be achieved with a capacitive on-chip matching network. The voltage amplitude at the IC is given by [15]

$$V_{IC} = \sqrt{\frac{2|Z_{IC}|^2}{Re(Z_{IC})} \tau_{ra-IC} P_L} \tag{3}$$

where $\tau_{ra\text{-}IC}$ is power transmission coefficient determined by the antenna and IC input impedances Z_{ra} and Z_{IC}, respectivly.

III. External Transmit Antenna

An external electric field generates currents in the dielectric human body causing temperature increase. Hence, power transfer via magnetic field is a favorable approach to the wireless powering of implanted devices. Prior research has shown that for a mm-size loop, implanted on top of the brain beneath the skull, the optimum frequency for wireless power transfer lies between 100 MHz and 1GHz [15]. The geometry of the transmitting loop should be optimized to have best link power efficiency with the implant antenna at a few 100 MHz. However, it is not enough to optimize the loop geometries for maximal link power efficiency only. Indeed, transmit loop geometry should provide low near electric field and high link power efficiency simultaneously: this means low SAR and efficient wireless power transfer between the transmitting and the implant loops. There are different ways to decrease SAR level and electric field hot spots in the tissues; partitioning the transmit loop into segments to produce uniform electric field [16-17], tilting the loop and receding the port from skin [18], and increasing the transmit loop-to-skin distance.

The aim of this study was to prove the applicability of two different implant loop antennas and compare their performance. Thus, in simulations and measurements we used a simple planar solid copper loop with 10 mm inner diameter, 3 mm trace width and 3.175 thick substrate (Rogers RT/Duroid 5880) (Figs. 4a and 5a). The dimensions of the transmit loop antenna were optimized for high coupling with the implant loops.

IV. Implant Antennas

From the clinical point of view, it would be best if the antenna did not increase the size of the implant significantly from that required by the neural sensor electrodes and the implant IC. Thus, neural sensors meant for localized neural recordings require mm-size antennas. Our previous research on implant loop size showed that three-dimensional structure provides wider current path and larger coupling area compared to planar loop with the same cross-sectional area [15]. Simulations with Man's Head Model confirmed that a 1-mm^3 cubic implant loop placed inside the CSF fluid achieves higher link power efficiency compared to a planar 2 × 2 mm^2 implant loop. At higher frequencies, it even performs as strongly as a 3 × 3 mm^2 implant loop (Fig. 2b). Consequently, three-dimensional structure achieves a cross-sectional area reduction of more than 75%. The improvement achieved with three-dimensional structure is even more evident when using less conductive or sub-skin-depth thin conductors. In these cases, the increase in trace width of a planar loop improves $G_{p,max}$ by reducing the current crowding, but this increases the loop size. This is not an issue in a three-dimensional implant loop, since it has wide enough current path. Moreover, cubic structure allows the insertion of magnetic core to further strengthen the magnetic field and thereby the inductive coupling.

As mentioned in the previous section, increasing transmit loop-to-skin distance decreases SAR in the tissues, but this is at the expense of lower link power efficiency. We investigated

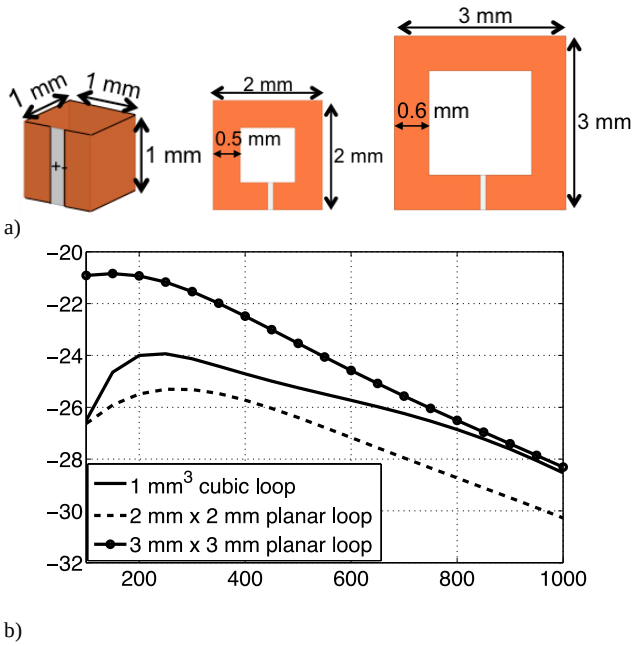

Fig. 2. (a) Cubic mm and planar implant antennas, (b) Maximum operating power gain (link power efficiency) of each implant antenna shown above.

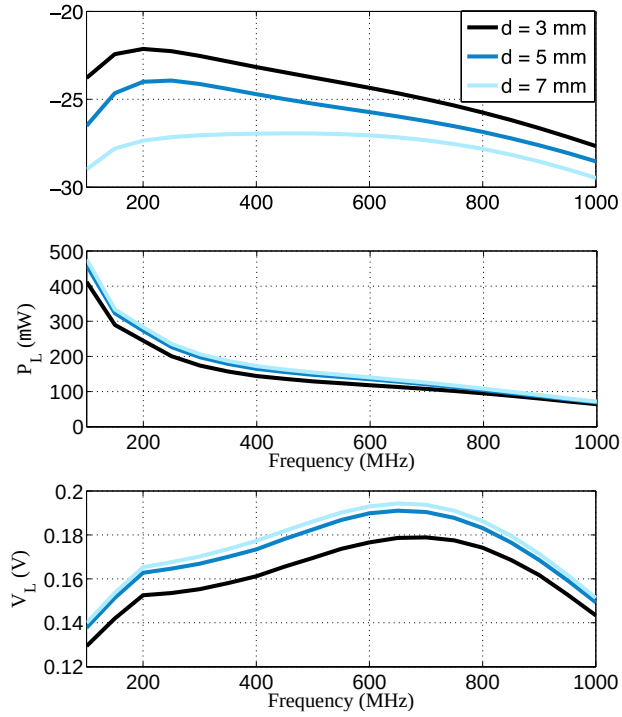

Fig. 3. Maximum operating power gain (link power efficiency), power available from the conjugate-matched cubic mm implant loop antenna for the IC and the corresponding voltage at the implant loop terminals with different transmit loop-to-skin distances *d*.

this trade-off by simulating 1 × 1 × 1 mm^3 copper loop immersed in the CSF fluid in Man's Head Model with the planar solid transmit loop placed in different distances *d* from the skin. Figure 3 shows the maximum operating power gain ($G_{p,max}$) between the loops in each case. In addition, it illustrates the power (P_L) delivered to a conjugate-matched implant IC and the corresponding voltage amplitude at its input with the maximum SAR compliant transmit power

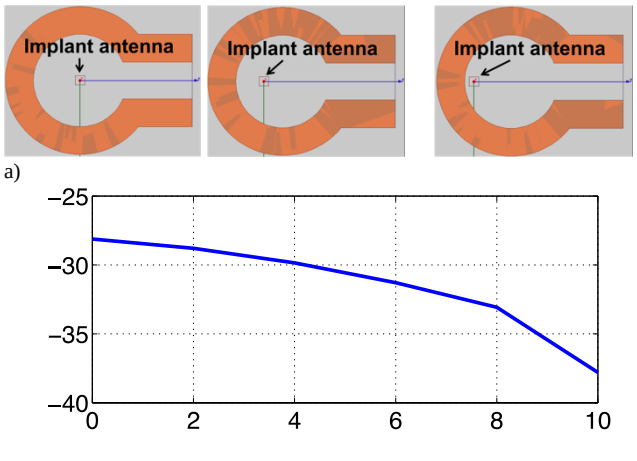

Fig. 4. (a) Antennas with centers perfectly aligned (shift = 0 mm), antennas with 2 mm lateral shift, antennas with 4 mm lateral shift, (b) Link power efficiency with respect to lateral misalignment.

($P_{t,max}$). The shown parameters were computed from Equations 1, 2 and 3. The results confirm that increase in d reduces SAR (which allows higher $P_{t,max}$) and $G_{p,max}$. This means that reduced link power efficiency could be compensated by increasing the transmission power, but considering that in a practical system the transmitter would be a mobile device, this would come at the expense of reduced battery-life. In view of this, d = 5 mm appears to be a suitable distance, because compared with distance d = 7 mm, similar voltage V_L and power P_L are achieved with much higher link efficiency $G_{p,max}$. Thus, the 1-mm^3 copper implant loop supplies 100s of microwatts of power to the implant IC, and generates 150−200 mV of voltage at the IC terminals (Fig. 3). Even though the 1-mm^3 implant loop is classified as a very small loop antenna, according to these results, it could power the neural recording IC presented in [10] with up to 92 channels.

Best coupling is achieved when the transmit and the implant antennas are perfectly aligned while any lateral misalignment decreases the link power efficiency. Figure 4 illustrates the effect of lateral misalignment of antennas on $G_{p,max}$, when the 1-mm^3 copper implant loop was immersed in CSF fluid in the Man's Head Model. The transmit loop antenna was placed 5 mm above the head. A center shift of 4 mm decreases $G_{p,max}$ only 18% (Fig. 4). Thus, the link power efficiency of the system is not highly sensitive to lateral misalignment. The effect of lateral misalignment of loops would be improved if the external transmit antenna was bigger in size. As an example of bigger transmit antenna, we can mention the wearable transmit antennas reported in [19]. The wearable transmit antennas have an inner diameter of 26 mm, which allow much more lateral misalignment.

V. Fabrication and Measurement

A. *Cubic 1 mm^3 Copper Implant Antenna*

In previous Section and in [15], we presented an analysis on the performance of planar and three-dimensional implant loop antennas. The aim of this study is to prove their feasibility

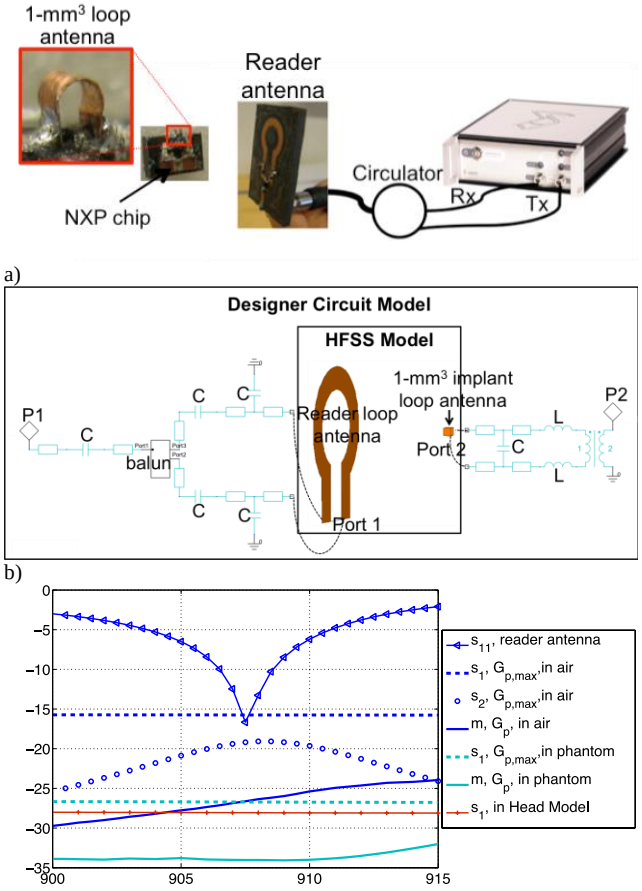

Fig. 5. (a) Wireless measurement system, reader and cubic mm implant antenna prototypes, (b) Simulation model of the whole communication link. Reader and implant loop antennas in HFSS model are dynamically linked to the components in Designer environment through Port 1 and Port 2, (c) Measurement and simulation results. In legend, subscript 1 refers to the simulated maximum operating power gain between the reader and the implant loop ports (Port1 and Port 2), subscript 2 refers to the simulated maximum operating power gain between the reader antenna matching circuit port, P1, and implant antenna port, Port 2, "s" stands for simulation and "m" for measurement.

through fabrication and measurements. Thus, we fabricated a 1×1×1 mm^3 copper loop equipped with an RFID tag IC (NXP UCODE G2iL) to create a backscattering tag for wireless testing (Fig. 5a). The IC supports ISO 18000-6C standard used in the RFID systems operating within the regionally regulated sub-bands of the global 840-960 MHz UHF RFID band. The cubic copper loop was made of 0.05 mm thick copper plate and it was attached to the NXP chip via a small test board, which conjugate matches the input impedance of the implant antenna to the input impedance of the chip. To avoid coupling of the matching circuit (MC) to the reader antenna, we tried to make it as small as possible. The resulted MC contains a parallel capacitor and two series inductors (Fig. 5b). The used reader loop antenna has a matching circuit, which converts its input impedance to 50 Ω at 907.5 MHz. A surface mount balun was used to properly convert the differential port of the reader loop antenna to single ended port (Fig. 5b). The matching circuits were designed using circuit design software Ansys Designer v.8.

In the wireless testing, we have used Voyantic Tagformance RFID measurement system. The measurement was based on ramping down the output power of the reader during the interrogation of the backscattering tag based on the 1×1×1 mm^3 copper loop. The lowest output power (threshold power: P_{th}) at which the tag responded remained readable. From the manufacturer's data we know the activation power of the IC: P_{ic0} = –18 dBm (15.6 μW). With this information, we computed the operating power gain (the ratio of the power delivered to the IC to the power entering the matching circuit of the transmitting antenna) of the wireless link from

$$G_p = \frac{P_{ic0}}{P_{th} G_{t,cable}}, \quad (4)$$

where $G_{t,cable}$ is the transducer power gain of the cable connecting the Tagformance output and the transmitting antenna (Fig. 5a). During the measurement, the distance between the backscattering tag and the transmitting antenna was set to 16 mm, which is the same as the implant-transmitter separation in the Man's Head Model in simulations.

For the judicious comparison between the simulation and measurement, we implemented the simulation model shown in Fig. 5b, which includes also the matching circuits present in the wireless testing. The lumped components and baluns were modeled in circuit solver Ansys Designer, which was dynamically linked to the electromagnetic fields solver HFSS through ports 1 and 2 sketched in Fig. 5b. Measurement and simulation results are shown in Fig. 5c.

As the measured S_{11} of the reader antenna shows (Fig. 5c), the reader antenna is matched at 907.5 MHz. Thus, the measured operating power gain G_p computed using (4) is reliable only in the surroundings of this frequency. Based on the HFSS simulation results, maximum operating power gain between the cubic mm loop port and reader loop port ($G_{p,max}$) is approximately −15.7 dB. To see the insertion loss of the reader antenna MC, we simulated $G_{p,max}$ between the implant loop port and the reader antenna MC port (graph 'S_2, $G_{p,max}$, in air' in Fig.5c). In this case, the implant loop is assumed to be perfectly matched and hence its matching does not affect the link efficiency. At the matched frequency of 907.5 MHz, $G_{p,max}$ is more than 3 dB lower than the $G_{p,max}$ between the loop antenna ports. This means that the reader antenna MC has an insertion loss of approximately 3 dB. On the other hand, the measured operating power gain G_p computed using (4) is approximately 11 dB lower than the simulated link power efficiency between the loop antenna ports. If 3 dB loss is caused by the reader antenna MC, 8 dB remains to be the insertion and matching loss of the implant antenna MC. Implant antenna MC could be further improved, but this would require bigger board and this would increase the coupling risk of the implant MC to the reader antenna.

The backscattering implant loop was also measured in human-head equivalent liquid phantom. The liquid phantom was made of water, sugar, and salt. Electrical properties of the liquid were adapted to mimic human head at 900−915 MHz using the recipe studied in [20]. We followed the dielectric properties in IEEE standard for head at 900 MHz (ε_r = 41.5 and σ = 0.97). First, we mixed sugar to water to lower the

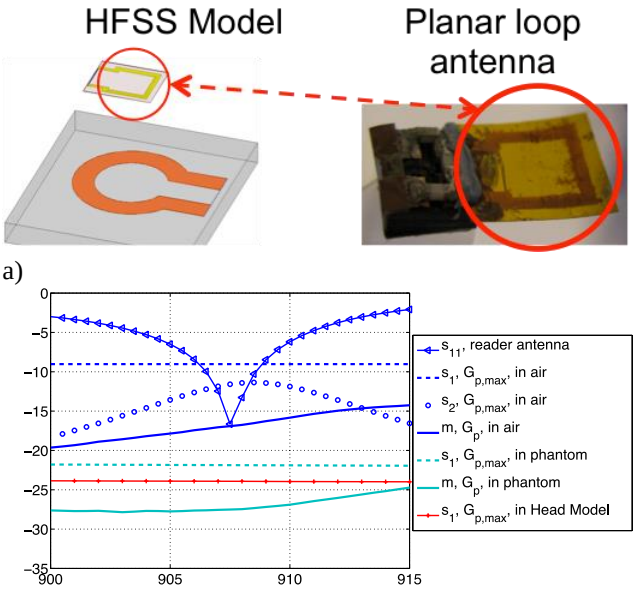

b)

Fig. 6. (a) Simulation model and implant antenna prototype, (b) Measurement and simulation results. In legend, subscript 1 refers to the simulated maximum operating power gain between the reader and the implant loop ports, subscript 2 refers to the simulated maximum operating power gain between the reader antenna matching circuit port and implant antenna port, "s" stands for simulation and "m" for measurement.

permittivity of water to the desired value. Then we added salt to increase the conductivity of solution. During the mixing, we monitored the dielectric properties of the solution using Agilent's 85070E Dielectric Probe Kit. In measurements, the backscattering 1-mm^3 implant antenna was immersed 11 mm beneath the liquid surface, and the reader loop antenna was placed 5 mm above the liquid surface. These distances correspond with the distances in the Man's Head Model. Before immersion, the implant antenna test board was coated with a thick Styrofoam layer and Blue-Tack to avoid impedance mistuning when the whole fixture was immersed in the liquid. In air measurement showed no effect from the coating layers. The measured *in phantom* operating power gain (G_p) is 7.3 dB lower than the simulated *in phantom* maximum operating power gain between the antenna ports (graph 'S_1, $G_{p,max}$, in phantom' in Fig. 5c). Hence, here 7.3 dB mismatch and insertion loss is detectable in the antenna test boards. This is lower than for *in air* case, because when placed in liquid resistance of the loop antenna increases increasing the frequency bandwidth of its matching circuit and improving the matching. According to the measurement results, at 907.5 MHz, the reader antenna transmit power is 20.1 mW (-18 dBm – (-34.03 dB) – 3 dB = 13.03 dBm). At this frequency, the maximum allowed transmit power computed using (1) is 50 mW. Thus, the IC activates with a transmit power which is 30 mW less than the maximum allowed transmit power, even though the implant loop MC has more than 4 dB insertion and matching loss. Thus, the cubic mm loop is able to power an IC with -18 dBm sensitivity without violating SAR limits. In addition, the simulated $G_{p,max}$ in the Man's Head Model (graph 'S_1, $G_{p,max}$ in Head Model' in Fig. 5c) is near the $G_{p,max}$

between the antenna ports when using liquid phantom (graph 'S_1, $G_{p,max}$ in phantom' in Fig. 5c). This means that at least from the link efficiency point of view, liquid phantom models human head appropriately.

B. *Ink-Jet Printed Gold Implant Antenna*

Extremely thin and flexible implant antenna conforming to the cortex is suitable for BMI applications, which require bigger neural sensors for recording neural data from a larger area. Hence, we also fabricated and measured wirelessly a flexible planar implant loop. Printable electronics provide means for simple deposition conductive patterns to a variety of substrates. Aiming to create biocompatible implant antennas, we fabricated the 6.5 × 6.5 mm^2 implant loop designed in [4] using ink-jet printing gold nanoparticle ink Harima Gold Nanopaste (Model: NPG-J). The shape of the antenna was ink-jet printed on 50 µm thick Kapton (Dupont Type 100 HN Film), which is also a biocompatible material. In contrast to the microfabrication of the antenna in a custom MEMS process [4], the ink-jet fabrication is a much simpler procedure where we used Dimatrix DMP-2800 series table-top printer. The implant antenna comprises 16 printed layers and has a sheet resistance of 0.35 Ω/□ (Fig. 6a). In the printing process, sintering was done after printing every 4 layers [21]. The fabricated loop was connected to RFID IC chip through a small matching circuit (Fig. 6a). Also here we tried to design as small matching circuit as possible to avoid possible coupling of it to the reader antenna. The designed matching circuit contained two series inductors. The backscattering gold planar loop was measured both in air and in the liquid phantom in the same manner as explained in Section V.A. Comparing the measured *in air* operating power gain G_p and the simulated *in air* link power efficiency $G_{p,max}$ between the antenna ports (graph 'S_1, $G_{p,max}$, in air' in Fig. 6b), we can detect 8 dB mismatch and insertion loss due to antenna test boards at 907.5 MHz. With 3 dB loss in the reader antenna test board, the implant antenna test board has 5 dB insertion and matching loss. Also here, when immersed in liquid phantom impedance matching in the implant antenna side improves. (Fig. 6b). According to the in liquid measurement results, at 907.5 MHz, the IC turns on with a reader loop transmit power of 4.5 mW (-18 dBm – (-27.52 dB) – 3 dB = 6.52 dBm). This is only 15.5 % of the maximum allowed transmit power computed using (1). In addition, simulations predict −24 dB link power between the gold implant antenna and the reader antenna when using Man's Head Model. The achieved $G_{p,max}$ corresponds with a $P_{t,max}$ of 29 mW. Thus, with perfect impedance matching and a transmit power of 29 mW, 118 µW could be delivered to the implant IC at 907.5 MHz. Although the ink-jet printed gold pattern is less conductive than bulk copper, the planar implant antenna is capable of providing high power to the implant IC.

Following the idea of creating three-dimensional loop antenna, we wrapped a sheet of ink-jet printed gold conductor on Kapton into a cylinder with the radius of 1 mm. However, during testing we found that the printed layer was not ductile enough to allow wrapping with the required small curvature radius: after wrapping the DC resistance of the printed conductor sheet had almost doubled leading to inferior RF performance. This was attributed to micro-cracks caused by the wrapping.

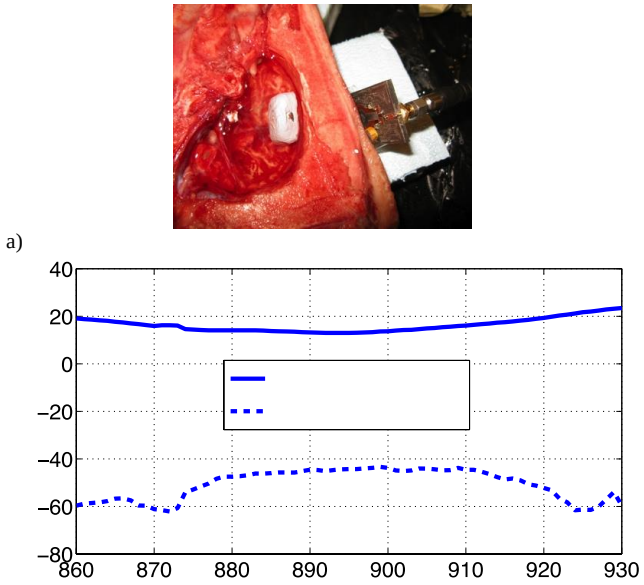

Fig. 7. (a) Measurement setup in pig's head, (b) Measured transmitted and backscattered power at the reader antenna matching circuit port.

C. *Porcine Measurements*

To further ensure the applicability of the designed loops in real biological environment, we also did measurements using the head of a post-mortem pig. The pig was 5-6 month old. Authors in [22] conducted measurements of dielectric parameters of pig biological tissues at different ages, re-confirming the age-dependence of dielectric characteristics of animal tissues. They also studied the correlation between the animal dielectric parameters and human dielectric parameters. According to this study, dielectric parameters of the pig we used correspond best with the dielectric parameters of an 11-13 years old human.

The pig's head used in the experiments was halved and the brain was removed from its skull. We filled the skull with Satimo's Head Liquid and immersed the implant loop in the liquid so that it touched the skull (Fig. 7a). The reader loop antenna was placed 5 mm away from the skin. The implant loop was aligned to the center of the reader loop for best magnetic coupling. The approximate thicknesses of the bone, fat and skin layers present in the power path were 20 mm, 5 mm, and 2 mm, respectively.

A backscattering cubic 1 mm^3 copper implant antenna was measured wirelessly when it was placed in the pig's head (Fig. 7a). During measurements, implant antenna test board was coated with a thick Styrofoam layer and Blue-Tack to avoid impedance mistuning when the whole fixture was immersed in the liquid. Testing in air with and without the coating showed that it did not influence the impedance matching. As Fig. 7b shows, we were able to communicate wirelessly with the backscattering implant equipped with the 1 mm^3 loop. Figure

7b illustrates the minimum transmit power, which turned on the RFID IC in the implant and the corresponding backscattered signal power received by the reader unit. According to the measurement results, at 907.5 MHz, a minimum transmit power of 14.28 dBm (26.8 mW) was required to turn on the NXP chip. The NXP chip requires −18 dBm (15.8 μW) of continuous RF power to establish the required DC supply for the circuitry. At this frequency, the power backscattered from the implant was −42.91 dBm (51.2 nW). The backscattered power is still 10-to-20 dB higher than the receiver sensitivity in commercial off-the-shelf RFID readers, while specialized equipment can still achieve better sensitivities. At this stage of testing, the implant antenna was, however, mounted on a larger test board compared to the one presented in Section V.A. In the future research one goal will be to minimize the test boards further to remove the possibility of any additional coupling through them. However, this is one of the first demonstrations of the wireless power and data telemetry with a real backscattering microsystem in a biological environment through a miniature antenna with size of only 1 mm^3. Here, it should also be noted that the biological channel in the test was in fact much longer than that it would be in human.

VI. Conclusion

We studied the feasibility of mm-size loop antennas in wireless powering of an implantable backscattering microsystem to demonstrate the applicability of this technology in a wireless BMI system. We presented the design and measurement of a miniature backscattering device based on a 1×1×1 mm^3 loop connected with an RFID IC and analyzed in detail the performance of implant loop antennas in considering the loop size and the conductor material type. The simulation results of the 1×1×1 mm^3 loop were validated through measurements in a human head equivalent liquid phantom and in the head of a post-mortem pig. The measurement in the liquid phantom showed the IC turns on with a transmit power of 20.1 mW, which is 30 mW lower than the maximum allowed transmit power restricted by SAR regulations. Porcine measurement results showed that a minimum transmit power of 26.8 mW was required to turn on the NXP chip at 917.5 MHz. Finally, we tested another backscattering tag based on a planar 6.5 × 6.5 mm^2 loop, which was fabricated by ink-jet printing gold nanoparticles on a plastic film. This is a simple and extremely fast method for producing conductive patterns on a wide variety of platforms. Despite the limited conductivity of the ink-jet printed pattern compared to bulk metals, the printed loop can provide 118 μW power to the IC.

References

[1] J. M. Carmena, "Advances in neuroprosthetic learning and control," *PLoS Biol.*, vol. 11, no. 5, May 2013.

[2] J.L. Collinger, B. Wodlinger, J.E. Downey, W. Wang, E.C. Tyler-Kabara, D.J. Weber, A.J. McMorland, M. Velliste, M.L. Boninger, A.B. Schwartz, "High performance neuroprosthetic control by an individual with tetraplegia," *Lancet*, vol. 381, no. 9866, pp. 564-557, Dec. 2012.

[3] J.M. Rabaey, "Brain-machine interfaces as the new frontier in extreme miniaturization," in *Proc. ESSDERC*, Helsinki, Finland, 2011, pp. 19-24.

[4] T. Björninen, R. Muller, P. Ledochowitsch, L. Sydänheimo, L. Ukkonen, M.M. Maharbiz, J.M. Rabaey, "Design of wireless links to implanted brain-machine interface microelectronic systems," *IEEE AWPL*, vol. 11, pp. 1663-1666, Jan. 2013.

[5] W. Wattanapanitch, R. Sarpeshkar, "A Low-Power 32-Channel Digitally Programmable Neural Recording Integrated Circuit," *IEEE Tran. Biomed. Circ. Syst.*, vol.5, no.6, pp.592, 602, Dec. 2011.

[6] K. Matsushita, M. Hirata, T. Suzuki, H. Ando, Y. Ota, F. Sato, S. Morris, T. Yoshida, H. Matsuki, T. Yoshimine, "Development of an implantable wireless ECoG 128ch recording device for clinical brain machine interface," *IEEE EMBS*, Osaka, Japan, 3-7 July 2013, pp.1867−1870.

[7] F. Zhang, A. Mishra, A.G. Richardson, B. Otis, "A Low-Power ECoG/EEG Processing IC With Integrated Multiband Energy Extractor," *IEEE Trans. Circ. Syst.*, vol.58, no.9, pp.2069−2082, Sept. 2011.

[8] K.W. Cheng, X. Zou, Z. Chen, R.F. Xue, J.H. Cheong, L. Yao, H.K. Cha, S.J. Cheng, P. Li, L. Liu, L. Andia, C.K. Ho, M.Y. Cheng, Z. Duan, R. Rajkumar, Y. Zheng, W.L. Goh, Y. Guo, G.S. Dawe, W.T. Park, and M. Je, "100-channel wireless neural recording system with 54-Mb/S data link and 40%-efficiency power link," *IEEE ASSCC*, Kobe, Japan, Nov. 12-14, 2012.

[9] W.S. Liew, X. Zou, L. Yao, Y. Lian, "A 1-V 60-mu W 16-channel interface chip for implantable neural recording," in Proc. *IEEE CICC*, San Jose, CA, USA, Sept. 13−16, 2009, pp. 507–510.

[10] R. Muller, S. Gambini, J.M. Rabaey, "A 0.013 mm^2, 5 μW, DC-Coupled Neural Signal Acquisition IC With 0.5 V Supply," *IEEE SCC*, vol.47, no.1, pp.232−243, Jan. 2012.

[11] D. A. Borton, M. Yin, J. Aceros, A. Nurmikko, "An implantable wireless neural interface for recording cortical circuit dynamics in moving primates", *J. Neural Eng.*, vol. 10, no. 2, Feb. 2013.

[12] Z. Xiao, C. M. Tang, C.M. Dougherty, R. Bashirullah, "A 20μW neural recording tag with supply-current-modulated AFE in 0.13μm CMOS," in *Proc. ISSCC*, San Francisco, CA, USA, Feb. 7−11, 2010, pp.122-123.

[13] H.N. Schwerdt, J. Chae, F.A. Miranda, "Wireless performance of a fully passive neurorecording microsystem embedded in dispersive human head phantom," in *IEEE APS Symp. digest*, July 8-14, 2012, Chicago, IL, USA.

[14] R. Sarpeshkar, "*Ultra Low Power Bioelectronics: Fundamentals, Biomedical Applications, and Bio-Inspired Systems*," Cambridge University Press, New York, USA, 2011, pp. 459-463.

[15] E. Moradi, T. Björninen, L. Sydänheimo, L. Ukkonen, J. M. Rabaey, "Analysis of Wireless Powering of mm-Size Neural Recording Tags in RFID-inspired Wireless Brain-Machine Interface Systems," *IEEE RFID Conf.*, Orlando, FL, USA, April 30-May 2, 2013.

[16] E. Moradi, T. Björninen, L. Sydänheimo, L. Ukkonen, J. M. Rabaey, "Antenna Design for Implanted Tags in Wireless Brain Machine Interface System," *IEEE APS Symp. digest*, July 7-13, 2013, Orlando, Florida, USA.

[17] E. Moradi, T. Björninen, L. Sydänheimo, J. M. Carmena, J. M. Rabaey, L. Ukkonen, "Measurement of Wireless Link for Brain Machine Interface Systems Using Human Head Equivalent Liquid," *IEEE AWPL*, vol. 12, pp. 1307-1310, Sept. 2013.

[18] T. Björninen, E. Moradi, L. Sydänheimo, J. M. Carmena, J. M. Rabaey, L. Ukkonen, "Electromagnetic Modelling and Measurement of Antennas for Wireless Brain-Machine Interface Systems," *IMWS Bio*, Singapore, Dec. 9-11, 2013.

[19] S. Amendola, E. Moradi, K. Koski, T. Björninen, L. Sydänheimo, L. Ukkonen, J. M. Rabaey, Y. Rahmat-Samii, "Design and optimization of mm-size implantable and wearable on-body antennas for Biomedical systems", *EUCAP*, April 6-11, 2014, Hague, Netherlands.

[20] G. Hartsgrove, A. Kraszewski, and A. Surowiec, "Simulated biological materials for electromagnetic radiation absorption studies," *Bioelectromagnetics*, vol. 8, no. 1, pp. 29–36, 1987.

[21] E. Moradi, S. Amendola, T. Björninen, L. Sydänheimo, L. Ukkonen, J. M. Carmena, J. M. Rabaey, "Wireless testing of ink-jet printed mm-size gold implant antennas for brain-machine interfaces," *IEEE APS Symp. Digest*, July 6-12, 2014, Memphis, Tennessee, USA, submitted.

[22] A. Peyman, C. Gabriel, E. H. Grant, G. Vermeeren, L. Martens "Variation of the dielectric properties of tissues with age: the effect on

the values of SAR in children when exposed to walkie–talkie devices," *Physics in Medicine and. Biology*, vol. 54, pp. 227 – 241, 2009.